Far-Field Optical Control of a Movable Subdiffraction Light Grid

J. Girard,[1] G. Scherrer,[2] A. Cattoni,[3] E. Le Moal,[4] A. Talneau,[3] B. Cluzel,[2] F. de Fornel,[2] and A. Sentenac[1,*]

[1]*Institut Fresnel, CNRS, Aix-Marseille Université, Marseille, France*
[2]*LICB, CNRS, Université de Bourgogne, Dijon, France*
[3]*LPN, CNRS, Marcoussis, France*
[4]*ISMO, CNRS, Université Paris XI, Orsay, France*

(Received 3 July 2012; published 31 October 2012)

We demonstrate experimentally a subdiffraction light pattern, with a period down to 150 nm, at the surface of an optimized silicon nanostructured thin film. We show, using near-field and far-field characterization, that this subdiffraction pattern can be translated and rotated just by changing the illumination angle. The movable high frequency light pattern paves the way for subdiffraction resolution surface imaging microscopy without scanning near-field probes.

DOI: 10.1103/PhysRevLett.109.187404 PACS numbers: 78.67.Pt, 42.30.Ms, 42.79.Dj, 42.82.Et

There is currently a wealth of research on the design of structured surfaces which exhibit highly localized light spots when conveniently illuminated. The applications are numerous, from optical sensing to data storage via superresolution imaging. The chosen route to control the light field at the nanoscale often belongs to the plasmonic domain [1] and many studies were devoted to the properties of metallic nanostructures supporting localized [2,3] and/or extended plasmons [4,5].

Yet, the experimental achievement of these promising approaches is still below what is required for practical subdiffraction optical imaging. Basically, if the spots are significantly under the diffraction limit, they cannot be moved continuously over areas large enough for convenient imaging [2,3]. Conversely, when the spots can be moved continuously, they are barely below the diffraction limit [4]. This difficulty stems from the fact that the highly subdiffraction spots are obtained through the excitation of localized modes that are bound to metallic particles, while the movable spots are obtained through the interference of extended plasmons [4,5], the wave numbers of which being close to that of free-space, $k_0 = 2\pi/\lambda$, where λ is the illumination wavelength.

To circumvent these issues, another solution relying on the high refractive index of semiconductors can be considered. Indeed, semiconductor thin films support guided modes with wave number k_{mode} much higher than k_0. Although these high frequency modes suffer from strong absorption losses in the optical regime, theoretical studies have shown that they can be excited from free-space using grating couplers and manipulated to form movable subdiffraction spots [6] or subdiffraction light grids [7]. In this work, we provide the first experimental demonstration that a significantly subdiffraction periodical light pattern can be translated and rotated at the surface of a nanostructured semiconductor thin-film just by changing the illumination angle.

Following the approach depicted in [7], we designed a multilayer grating made of a glass substrate (a cover-slip adapted to microscope objectives with refractive index $n_{\mathrm{glass}} \approx 1.5$) and a 33 nm thin layer of amorphous silicon (a-Si, $n_{a\mathrm{Si}} \approx 4.15 + i0.091$). At $\lambda = 633$ nm, such a multilayer supports a TE lossy guided mode with wave number $k_{\mathrm{mode}} \approx 2.43k_0$. The choice of the amorphous silicon layer thickness resulted from a compromise between the mode spatial frequency and the deterioration of the resonance and of the light transmission which both increased with the layer thickness. An optimized grating coupler with a triangular lattice of cylindrical holes (diameter 110 nm, depth 28 nm) with pitch $d \approx 210$ nm was etched in the silicon layer, as depicted in Figs. 1(a) and 1(b). To avoid any imaging artifact due to the topography, the surface of the grating was flattened using a fluid resin ($n_{\mathrm{resin}} = 1.5$) that filled the holes and formed a 20 nm film above the grating once cured. To excite the guided mode, a s-polarized incident plane wave (the electric field is parallel to the (x, y) plane) coming from the substrate with in-plane wave vector $\mathbf{k}_{\mathrm{inc}} = n_{\mathrm{glass}}k_0 \sin\theta\mathbf{y}$ is sent at an angle $\theta = 65°$ such that $|\mathbf{k}_{\mathrm{inc}} - K\mathbf{y}| \approx k_{\mathrm{mode}}$, where $-K\mathbf{y} = (2\pi/d) \times (3/\sqrt{2})\mathbf{y}$ is the $(0, -1)$ grating diffraction order. Under this illumination configuration, the $(0, -1)$ grating evanescent order has the spatial frequency of the guided mode and its modulus $|A_{0,-1}|$ is comparable to that of the specularly transmitted (0,0) order $|A_{0,0}|$ and much bigger than all the others. As a result, the field intensity at the resin-air interface can approximately be written as,

$$|\mathbf{E}|^2(x, y) \approx |A_{0,0}|^2 + |A_{0,-1}|^2 + 2|A_{0,0}A_{0,-1}| \cos[\Psi - Ky], \qquad (1)$$

where Ψ is the relative phase between $A_{0,0}$ and $A_{0,-1}$. The grating is optimized to get $\Psi \approx 90°$ so that the sinusoidal light grid is displaced by half a period when the incident polar angle is changed to $-65°$. The rotation by 60° and 120° of the light grid is obtained by illuminating the grating under the other equivalent directions of the triangular lattice.

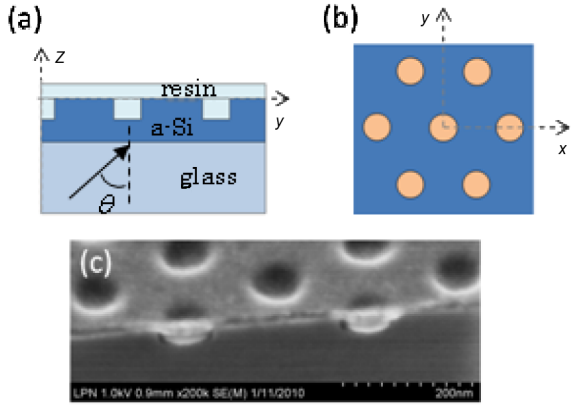

FIG. 1 (color online). Schematic views of the grating and of the illumination configuration. (a) Vertical view. (b) Top view. (c) Electronic image of a similar grating manufactured on a silicon substrate to permit a clean cleaving. The thin resin film that fills the holes is clearly visible.

The nanostructured substrate was realized using standard nanotechnology process. The a-Si layer was deposited by PECVD on a microscope cover slip and patterned through a positive resin mask formed by e-beam lithography. A dedicated SF6-CHF3 etching process was developed to produce smooth and vertical hole side walls in the silicon layer. The grating was embedded in resin (MMS10—Amo GmbH) using Degassing Assisted Patterning [8]; see Fig. 1(c).

In order to reveal the subdiffraction periodic light grid, the latter was directly probed with a home-built scanning near-field optical microscope (SNOM) [9,10] operating in collection mode. The nanostructured cover slip was illuminated by an s-polarized collimated laser beam (He-Ne, $\lambda = 633$ nm) through a hemicylindrical glass prism along the y axis of the grating and under $\theta = 65°$. Thanks to piezoelectric stages with a shear-force feedback, a near-field probe was scanned in the (x, y) plane at a fixed distance from the air-resin interface (about 10 nm). The near-field probe consists in a pulled silica optical fiber with an approximately 20 nm apex which locally detects the electric field intensity surrounding the nanostructure. The light collected by the near-field probe was measured by a photomultiplier tube (R928 Hamamatsu) and the intensity map revealed a one-dimensional periodic pattern with period about 190 nm to be compared to the theoretical $d\sqrt{2}/3 \approx 182$ nm; see Fig. 2.

To demonstrate the translation of the light grid when the angle of incidence is switched from $\theta = 65°$ to $\theta = -65°$, the laser beam was split in two and sent successively towards the grating under $\theta = 65°$ and $\theta = -65°$. The acquisition procedure consisted in switching from one beam to the other for a given probe position. It appeared clearly that the black fringes of the one-dimensional periodic pattern (with period about 190 nm) were replaced by bright ones when the incidence angle was changed; see Fig. 3.

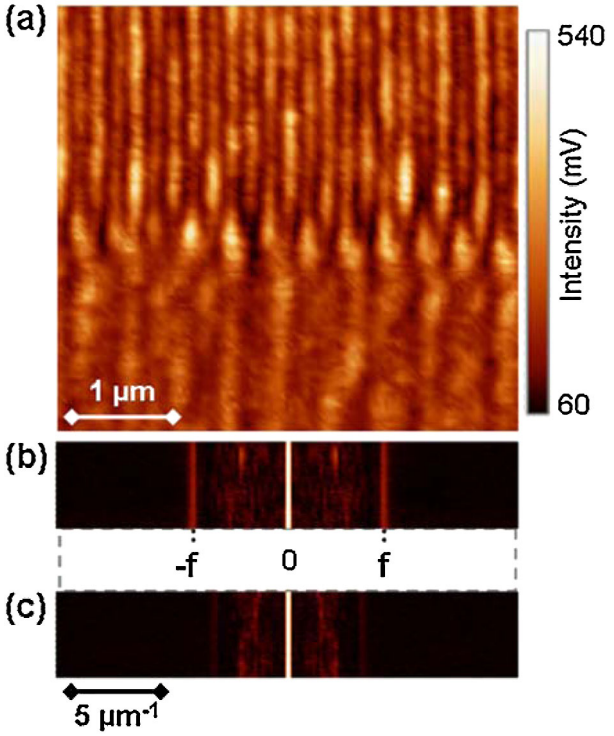

FIG. 2 (color online). (a) Near-field intensity map recorded partly above and partly outside the structured region of the substrate. The substrate is illuminated by a collimated beam directed in the (y, z) plane with polar angle $\theta = 65°$. The intensity above the grating displays a highly contrasted 1D periodic modulation. (b) Modulus of the 1D Fourier transform along the horizontal axis of the intensity recorded above the grating. The detected Fourier peaks correspond to a light grid with period about 190 nm (182 nm theoretically). (c) Modulus of the 1D Fourier transform along the horizontal axis of the intensity recorded outside the grating. One observes a weak modulation, with period about 245 nm, which corresponds to the interference of the incident beam with its unwanted reflection at the exit of the prism.

We also analyzed the intensity map which is obtained when the grating is illuminated simultaneously by both beams, Fig. 4. In this case, the intensity can be described by four cosine functions, corresponding to the interference between the two counter-propagative transmitted beams and the two counterpropagative excited guided modes, with angular frequencies, $2k_{\mathrm{inc}}$, K, K-$2k_{\mathrm{inc}}$, and $2K$-$2k_{\mathrm{inc}}$ corresponding to periods of 230, 182, 873, and 150 nm, respectively. As expected, the intensity spectrum measured above the grating displays four peaks corresponding reasonably to the theoretical frequencies. Even the smallest feature, the $2K$-$2k_{\mathrm{inc}}$ frequency, corresponding to a period about 150 nm ($< \lambda/4$) is successfully revealed. On the contrary, above the nonstructured region of the cover slip, the intensity spectrum displays only the frequency $2k_{\mathrm{inc}}$ corresponding to the standing-wave illumination pattern. To explain the minor differences between the measured frequencies and the theoretical ones (about 5%), we identified three main causes:

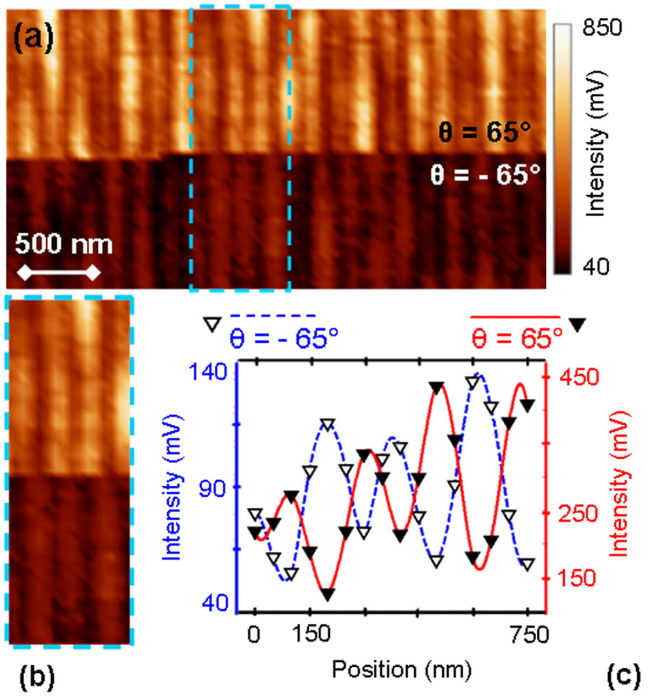

FIG. 3 (color online). Near-field intensity recorded above the structured region of the substrate when the illumination angle is switched from $\theta = 65°$ to $\theta = -65°$ during the same image acquisition. The black fringes are replaced by white fringes when the angle is changed. The lesser contrast observed for one illumination is explained by the asymmetry of the near-field probe, which does not behave in the same way when light comes from the right or from the left. (b) Zoom of the dashed zone in (a). (c) The experimental data from the $\theta = 65°$ and the $\theta = -65°$ parts of (b) are numerically averaged along the vertical axis of the fringes (see the plotted markers) and then interpolated. The resulting interpolations are shown and exhibit two sinusoidal-type curves shifted by half a period.

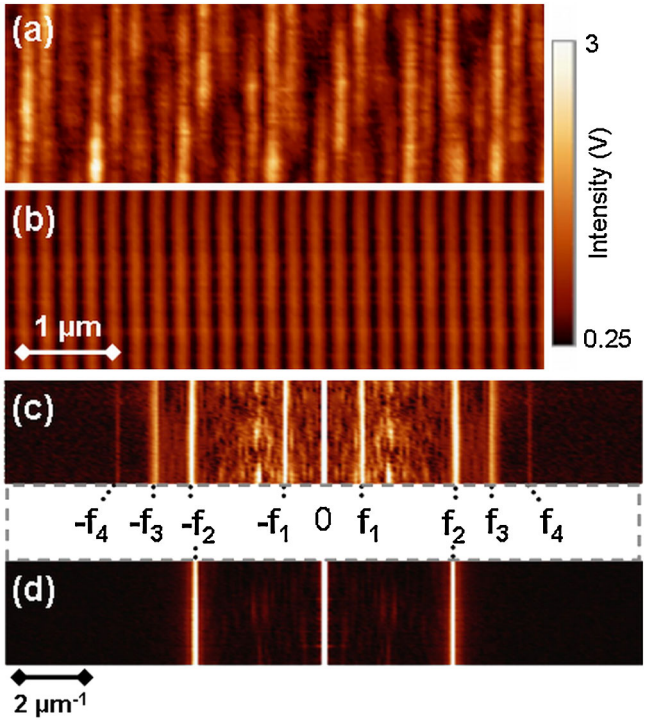

FIG. 4 (color online). (a) Near-field intensity recorded above the grating when the substrate is illuminated simultaneously by two interfering collimated beams under $\theta = 65°$ and $\theta = -65°$. The mixing between the incident standing-wave frequency and that of the grating yields a complicated 1D pattern. (b) Same as (a) but above a homogeneous region of the substrate. In this region, only the standing-wave incident pattern is visible. (c) Modulus of the 1D Fourier transform along the horizontal axis of (a): four main spatial frequencies (f_1, f_2, f_3, and f_4) emerge. The corresponding periods are about 830 nm (f_1), 243 nm (f_2), 190 nm (f_3), and 155 nm (f_4), to be compared to $2\pi[K - 2k_{\mathrm{inc}}] = 873$ nm, $2\pi/[2k_{\mathrm{inc}}] = 230$ nm, $2\pi/[K] = 182$ nm, and $2\pi/[2K - 2k_{\mathrm{inc}}] = 150$ nm. (d) Modulus of the 1D Fourier transform of (b): a single spatial frequency (f_2) is evidenced which corresponds to the period of the standing-wave illumination (230 nm theoretically and 249 nm measured). Note that (a) and (b) have the same size and color scale limits.

(i) the calibration of the piezoelectric stages relating to the near-field probe displacements, (ii) the incident angles sub-degree accuracy of the two incident beams, and (iii) the small discrepancies between the theoretical and experimental grating parameters.

We observe that the light pattern obtained at the surface of the grating with the two beams illumination exhibits an angular frequency K-$2k_{\mathrm{inc}}$ which is much smaller than k_0 and thus accessible to a far-field microscope.

To reveal this pattern, we covered the grating with a homogeneous thin layer of 24 nm fluorescent beads (Fluosphere, Invitrogen, crimson fluorescent) and placed the substrate in a home-built fluorescence microscope. Thanks to a glass transmission grating (holographic, 80 lines/mm) placed in a secondary image plane of the microscope and illuminated with a collimated laser beam (He-Ne, 633 nm), a sinusoidal light pattern (with period about 230 nm) was formed on the nanostructured substrate through a high numerical aperture objective (NA 1.49, CFI Apo TIRF 100x, Nikon). The orientation and position of the standing wave were controlled with translation and rotation of the transmission grating. As in conventional epifluorescence geometry, the fluorescence light was collected with the same objective, separated from the laser reflection with a dichroic mirror and a filter, and finally imaged on an EMCCD camera (Andor iXon 897).

We plot in Fig. 5(a) the fluorescence image of the nanostructured cover slip for one orientation of the standing-wave illumination. We first observe that, due to the resonance field enhancement, the fluorophore intensity is brighter above the grating region than above the nonstructured region. In the nonstructured region, the fluorescence intensity is roughly homogeneous. The small period of the incident standing-wave pattern is not visible. This is due to the fact that, because of the fluorescence Stokes shift, the detection frequency cutoff of the objective is

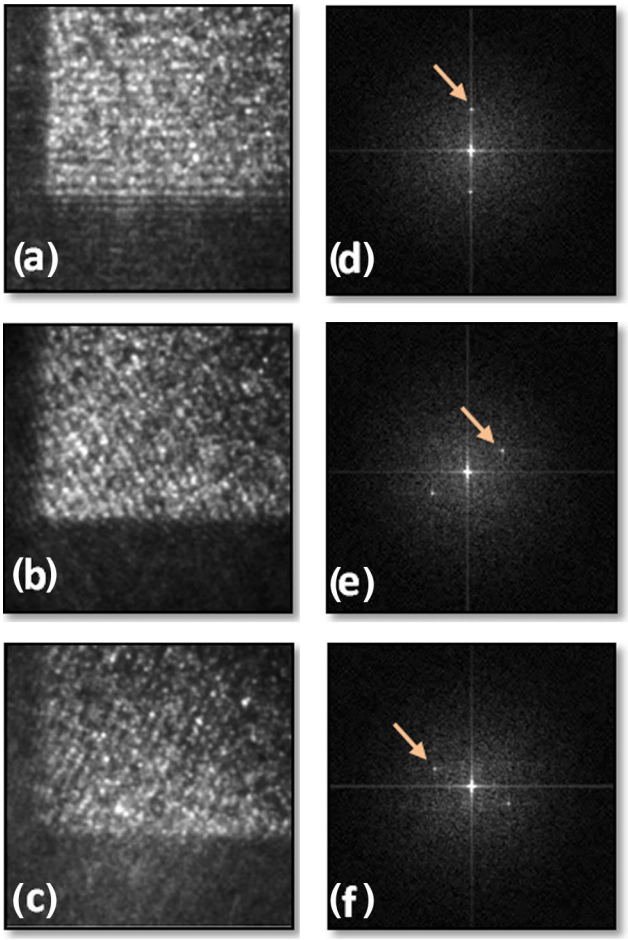

FIG. 5 (color online). Fluorescence intensity, imaged by a far-field microscope, of a monolayer of fluorescent beads deposited on the nanostructured substrate. The sample is illuminated by two interfering collimated beams as in Fig. 4. In the structured region of the substrate, the low frequency features of the near-field pattern (corresponding to K-$2k_{\mathrm{inc}}$) are detected. Outside the structured region, the fluorescence intensity is homogeneous, the illumination standing-wave pattern (with period about 230 nm) is not visible. (b),(c) same as (a) but the incident standing-wave has been rotated by $\pi/3$ and $2\pi/3$ respectively. (d),(e),(f) Modulus of the 2D Fourier transform of (a),(b),(c). The bright spots indicated by the arrows are a clear signature of the periodicity of the fluorescence signal above the grating. They correspond to sinusoidal patterns with period about 928 nm, to be compared to the theoretical period of 870 nm.

lower than the illumination cutoff. On the contrary, in the grating region, a one-dimensional low frequency periodic pattern, stemming from the interference between the guided modes and the incident standing waves, is clearly observed, Figs. 5(a) and 5(d). The measured period of about 928 nm is in reasonable agreement with the theoretical period of 873 nm. The discrepancy of 6% can be partly explained by the rather large imprecision on the incident angles (about $\pm 1°$).

In Figs. 5(a)–5(c), the fluorescence image of the grating under three different orientations of the illumination standing wave, corresponding to the three directions of the grating reciprocal triangular mesh, are displayed. As expected, we observe that the fluorescence pattern rotates with the illumination, Figs. 5(d)–5(f). We also checked that the periodic pattern above the grating moved accordingly when the illumination standing-wave was translated (not shown).

In conclusion, we have shown that a complex light grid with a period significantly smaller than the diffraction limit ($< \lambda/4$) can be translated and rotated at the surface of a periodically nanostructured substrate just by changing the incident angle. Even better results should be obtained by replacing amorphous silicon by less lossy, highly refracting, materials [11]. A promising application for these grating-substrates is superresolution surface imaging [7], especially in the framework of structured illumination microscopy [12,13] in which the sample is numerically reconstructed from a set of images obtained for various translations and rotations of a periodic illumination.

This work was partially funded by the French *Agence Nationale de la Recherche* under Contract No. ANR-08-NANO-P053-36 and by the Regional Council of Burgundy.

*Corresponding author: anne.sentenac@fresnel.fr

[1] D. Gramotnev and S. Bozhevolnyi, Nature Photon. **4**, 83 (2010).
[2] G. Volpe, S. Cherukulappurath, R. J. Parramon, G. Molina-Terriza, and R. Quidant, Nano Lett. **9**, 3608 (2009).
[3] M. Aeschlimann *et al.*, Proc. Natl. Acad. Sci. U.S.A. **107**, 5329 (2010).
[4] B. Gjonaj, J. Aulbach, P. M. Johnson, A. P. Mosk, L. Kuipers, and A. Lagendijk, Nature Photon. **5**, 360 (2011).
[5] Z. Liu, H. Lee, Y. Xiong, C. Sun, and X. Zhang, Science **315**, 1686 (2007).
[6] A. Sentenac and Patrick Chaumet, Phys. Rev. Lett. **101**, 013901 (2008).
[7] A. Sentenac, K. Belkebir, H. Giovannini, and P. C. Chaumet, J. Opt. Soc. Am. A **26**, 2550 (2009).
[8] A. Cattoni, A. Talneau, A.-M. Haghiri-Gosnet, J. Girard, and A. Sentenac, Microelectron. Eng. (to be published).
[9] L. Salomon, G. Bassou, H. Aourag, J. P. Dufour, F. de Fornel, F. Carcenac, and A. V. Zayats, Phys. Rev. B **65**, 125409 (2002).
[10] D. Brissinger, A. L. Lereu, L. Salomon, T. Charvolin, B. Cluzel, C. Dumas, A. Passian, and F. de Fornel, Opt. Express **19**, 17 750 (2011).
[11] R. W. Collins, A. S. Ferlauto, G. M. Ferreira, Chi Chen, Joohyun Koh, R. J. Koval, Yeeheng Lee, J. M. Pearce, and C. R. Wronski, Solar Energy Material and Solar Cells **78**, 143 (2003).
[12] R. Heintzmann and M. Gustafsson, Nature Photon. **3**, 362 (2009).
[13] E. Mudry, K. Belkebir, J. Girard, J. Savatier, E. Le Moal, C. Nicoletti, M. Allain, and A. Sentenac, Nature Photon. **6**, 312 (2012).